Giant Resistance Switch in Twisted Transition Metal Dichalcogenide Tunnel Junctions

Marc Vila[1, 2, *]

[1] *Materials Sciences Division, Lawrence Berkeley National Laboratory, Berkeley, California 94720, USA*
[2] *Department of Physics, University of California, Berkeley, California 94720, USA*

(Dated: June 24, 2024)

Resistance switching in multilayer structures are typically based on materials possessing ferroic orders. Here we predict an extremely large resistance switching based on the relative spin-orbit splitting in twisted transition metal dichalcogenide (TMD) monolayers tunnel junctions. Because of the valence band spin splitting which depends on the valley index in the Brillouin zone, the perpendicular electronic transport through the junction depends on the relative reciprocal space overlap of the spin-dependent Fermi surfaces of both layers, which can be tuned by twisting one layer. Our quantum transport calculations reveal a switching resistance larger than 10^6% when the relative alignment of TMDs goes from 0° to 60° and when the angle is kept fixed at 60° and the Fermi level is varied. By creating vacancies, we evaluate how inter-valley scattering affects the efficiency and find that the resistance switching remains large (10^4%) for typical values of vacancy concentration. Not only should this resistance switching be observed at room temperature due to the large spin splitting, but our results also show how twist angle engineering and control of van der Waals heterostructures could be used for next-generation memory and electronic applications.

Introduction — A two-level resistance switch is at the core of information storage and processing in current technologies, and continues to be nowadays a major field of research [1, 2]. Typically, this phenomenon is achieved in multilayer structures comprised of a metal-insulator-metal junction, with different mechanisms responsible for the resistance variation such as ferroelectric polarization [3, 4], spin-dependent tunneling [5–7] or ion migration [8, 9]. The high and low resistance states can be associated with a bit of information, and therefore, the larger the difference between them, the more reliably those states can be distinguished between each other. The resistance switching can be quantified as the change in percentage between the high (R_{high}) and low (R_{low}) resistance values,

$$R_{\text{sw}} = \frac{R_{\text{high}} - R_{\text{low}}}{R_{\text{low}}} \times 100\%. \tag{1}$$

In magnetic tunnel junctions, due to the spin-dependent transmission probability [10, 11], R_{low} and R_{high} correspond to metals with parallel and antiparallel magnetic orientations, respectively, and R_{sw} typically reaches values of few hundreds [12].

Although different physics govern the distinct types of switching devices, common challenges exist that limit their potential. Interface quality and scalabilty are major concerns, especially in ferroic systems where decreasing the system size may render the ordered phases more susceptible to thermal fluctuations [12–14] and interface details can impact the transport and polarization properties [4, 15, 16]. For that reason, two-dimensional materials have attracted a lot of attention as a way to circumvent those problems given their intrinsic low dimensionality and the ability to form pristine interfaces when stacked in van der Waals heterostructures [13, 17–20], and they have already shown exceptional switching capabilities of up to 10^6% [21–30]. Additionally, these layered heterostructures possess unique degrees of freedom such as their relative twist angle, and even though such angle can be harnessed to control transport properties [31, 32] or engineer electronic devices [33], experimental efforts so far have focused more on superconductivity [34–37], electronic correlations [38–42] or topological phases of matter [43–49].

Another recent improvement in the field of magnetic tunnel junctions has been the fact that momentum-dependent transmission between the different layers involved in the vertical transport [50, 51] could realize resistance switches in antiferromagnets. This is based on the relative orientation of the Néel vectors and therefore debunks the idea that only ferromagnets possess spin-filtering properties. The variety of antiferromagnetic orders range from collinear [52] and noncolinear [53–55] to nonrelativistic spin-split antiferromagnets [56, 57] (so-called altermagnets [58, 59]), and the generality of this momentum-dependent transmission is such, that it was also suggested for in-plane transport in transition metal dichalcogenide (TMD) monolayers [60] and twisted graphene multilayers between Cu or Ni [61]. This effect, however, does not need to be restricted to magnetic materials. Spin-dependent transmission could appear generally in systems possessing momentum-dependent spin splittings, such as materials with strong spin-orbit coupling (SOC) showing Rashba [62] or spin-valley locking [63]. Nevertheless, the switching between R_{low} and R_{high} is not straightforward, as the SOC strength and sign is usually fixed in a material in contrast to the magnetization or Néel vector.

In this Letter, we apply the concept of momentum-dependent transmission in tunnel junctions comprised of TMD monolayers to realize a resistance switch based on their valley-dependent spin splitting. The switching is achieved by twisting one of the layers by 60°, which ef-

fectively reverses its valley-dependent spin splitting resulting in a high resistance state. By employing quantum transport calculations with realistic parameters, we obtain $R_{\rm sw}$ larger than $10^6\%$ between twist angles $\theta = 0°$ and $\theta = 60°$. Such $R_{\rm sw}$ can also be attained at a constant relative angle of 60° with just tuning the Fermi level. Not only should the predicted effect be present at room temperature given the large spin-orbit splitting, but also the efficiency remains as large as $10^4\%$ for typical values of vacancy concentration, suggesting a very clear experimental signature that could be probed with recent methods of twist angle control [64–66].

One of the most widely known property of hexagonal TMDs is the spin-valley locking of the valence bands that produces an opposite spin splitting at K and K' valleys [63, 67, 68]. This is described by the effective SOC term $\Delta s\tau$, with 2Δ being the splitting, s the spin index (+1 and −1 for up and down spins, respectively) and τ the valley index (+1 and −1 for K and K', respectively). The splitting reaches up to few hundreds of meV, which means that each valley is fully spin polarized at low energies. In principle, the sign of the spin-valley locking $s\tau$ is fixed for a given material, and determines whether e.g. K valley is up or down spin-polarized. Nevertheless, since a symmetry operation applies to both real and reciprocal space, one can take a TMD bilayer and rotate only one of the layers with the result being two Brillouin zones twisted with respect to one another. Due to the three-fold rotation symmetry of TMDs, if the twist angle θ is 0° plus a multiple of 120°, the bilayer stack remains unchanged. However, for twist angles of 60° plus a three-fold rotation, K and K' are swapped and consequently the sign of $s\tau$ is effectively reversed, resulting in opposite spin splittings (between top and bottom TMDs) sharing the same momentum space in the common Brillouin zone. This procedure is illustrated in Fig. 1(a), and was used to control the excitonic properties in WSe_2 bilayers [69] and to generate a quantum anomalous Hall insulator in $MoTe_2/WSe_2$ heterobilayers [47].

If we now separate this bilayer with a thin insulating barrier like hexagonal boron nitride, the transport through the junction will just involve tunneling of TMD states between top and bottom layers. Therefore, the tunneling conductance or resistance will strongly depend on whether those states have the same or opposite spin polarization given by $s\tau$, akin to ferromagnetic tunnel junctions where that role is taken by the magnetization. In this way, when $\theta = 0°$, both TMDs have effectively the same $s\tau$ and the transport through the junction will show a low resistance state. In contrast, we expect a large resistance increase for $\theta = 60°$ due to swapping $s\tau$ in one of the layers. This idea is shown in Fig. 1(a) and is the core concept of our work, which we now substantiate with quantum transport numerical calculations.

Methodology — To calculate transport properties in a tunnel junction device, we implement the tight-binding

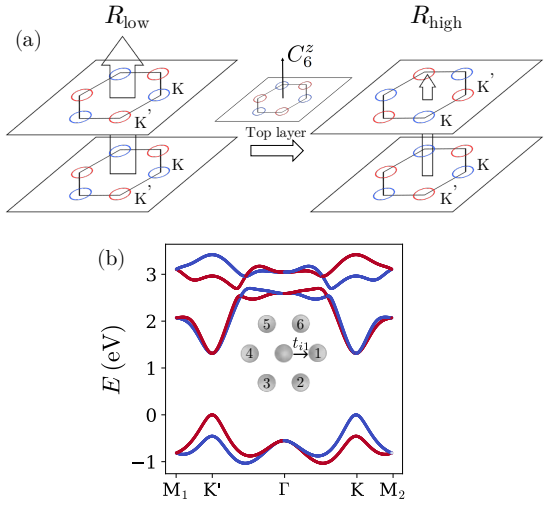

FIG. 1. (a) Schematics of the switching resistance based on twisted TMD tunnel junction, where the tunnel barrier has been omitted for clarity. When the spin-valley locking is the same in both layers, transport accros the junction leads to a low resistance state, $R_{\rm low}$. In contrast, rotating one of the layers by 60° (i.e. C_6^z operation) leads to an effective swapping of the spin-valley locking sign in that layer, which impedes vertical transport and results in a large resistance, $R_{\rm high}$. (b) Band structure of the tight-binding model Eq. (2) with the parameters of WSe_2 monolayer [72]. The zero energy is set at the valence band maximum. Inset: triangular lattice of the model with one of the nearest-neighbor hopping.

model of Ref. [70] in the Kwant transport package [71] and calculate the Landauer-Büttiker conductance. The Hamiltonian is written in the basis of d-orbitals and spin $\{(|d_z^2\rangle, |d_{xy}\rangle, |d_{x^2-y^2}\rangle) \otimes |\uparrow,\downarrow\rangle\}$ on a triangular lattice, and reads:

$$H = \left(\varepsilon_0 \sum_{i,s} c_{i,s}^\dagger c_{i,s} + \sum_{\langle i,j\rangle,s} c_{i,s}^\dagger t_{ij} c_{j,s}\right) \otimes s_0 + \left(\lambda L_z \sum_{i,s} c_{i,s}^\dagger c_{i,s}\right) \otimes s_z + +H.c.. \quad (2)$$

The first term is the onsite energy with value $\varepsilon_0 = (\varepsilon_1, \varepsilon_2, \varepsilon_2)$, the second term is the nearest-neighbor hopping and the third term is the on-site spin-orbit coupling with strength λ, which in this basis only the L_z component of the angular momentum operator is nonzero. Also, s_0 and s_z are the identity and z-Pauli matrices, respectively, acting on the spin and $c_{i,s}^\dagger$ ($c_{i,s}$) is the creation (annihilation) operator of an electron at site i with spin s. The hoppings follow the symmetries of the TMD monolayer's space group, i.e. defining the hoping t_{i1} as shown in the inset of Fig. 1(b), t_{i4} is obtained by a reflection on the x axis, and the remaining ones are obtained by three-fold rotations. The Fourier transform of the model

in Ref. [70] results in a hopping t_{i1} defined as:

$$t_{i1} = \begin{pmatrix} t_0 & t_1 & t_2 \\ -t_1 & t_{11} & t_{12} \\ t_2 & -t_{12} & t_{22} \end{pmatrix}. \quad (3)$$

For this work, we restrict ourselves to nearest-neighbor hoppings, as this is enough to capture the spin-valley physics of the valence band. Noting that our results are general for any TMD showing spin-valley locking, we focus here on WSe_2 because it has a large energy separation between the valence band maximum of the K, K' points and the Γ point. This is important as the bands at Γ point do not show spin-valley physics and would be detrimental for the resistance switching. The values of the parameters are reported in Table I of the supplemental material (SM) [72], and here we just note that both the hopping amplitudes and the spin-orbit strength are of the order of few hundreds of meV. In Fig. 1(b) we plot the band structure of such model for WSe_2, where the valley-dependent spin splitting in the valence band is clearly visible. Having the tight-binding for the TMDs, we now can model the tunnel junction device, which we schematically plot in Fig. 2(a). In what follows, we present results for WSe_2 using a tunnel barrier with the same lattice as the TMDs. In the SM [72], in addition to details of the junction implementation, we provide complementary results on other TMDs and barrier lattices to support the validity of our results.

Results — We plot in Fig. 2(b) the two-terminal resistance, obtained from inverting the Landauer conductance, as a function of energy for twist angles $\theta = 0°$ and $\theta = 60°$. As expected, the resistance for $\theta = 60°$, R_{60}, is considerably larger than that of aligned TMDs, R_0. Both resistances decrease with moving away from the valence band maximum because there are more states available for transport. However, around $E \sim -0.45$ eV, R_{60} starts dropping at a faster rate and becomes much more similar to R_0 after $E \sim -0.55$ eV. To help explain this effect, we plot the band structure of the valence band in the inset of Fig. 2(c). At $E \sim -0.45$ eV, the opposite spin band at each valley starts contributing to transport, thus reducing the resistance. However, the two Fermi surfaces at each valley are split and so the resistance remains relatively large. On the other hand, states at the Γ point appear at $E \sim -0.55$ eV, and since they have little to no spin splitting, the conduction becomes shunted and the resistance becomes almost as that of $\theta = 0°$.

From these resistances, we plot R_{sw} in Fig. 2(c), revealing a giant switching resistance larger than $10^6\%$ in a wide energy range. To compare such a value with state-of-the-art devices, we report experimental values of spin-based switching resistances in Table I. Our results exceedingly surpasses traditional magnetic tunnel junctions and competes well with recent experiments on two-dimensional ferromagnets [21, 25], with the advantage that these experiments requires the application of a magnetic field and that the presented SOC-based switching resistance is not limited to operate below a Curie temperature.

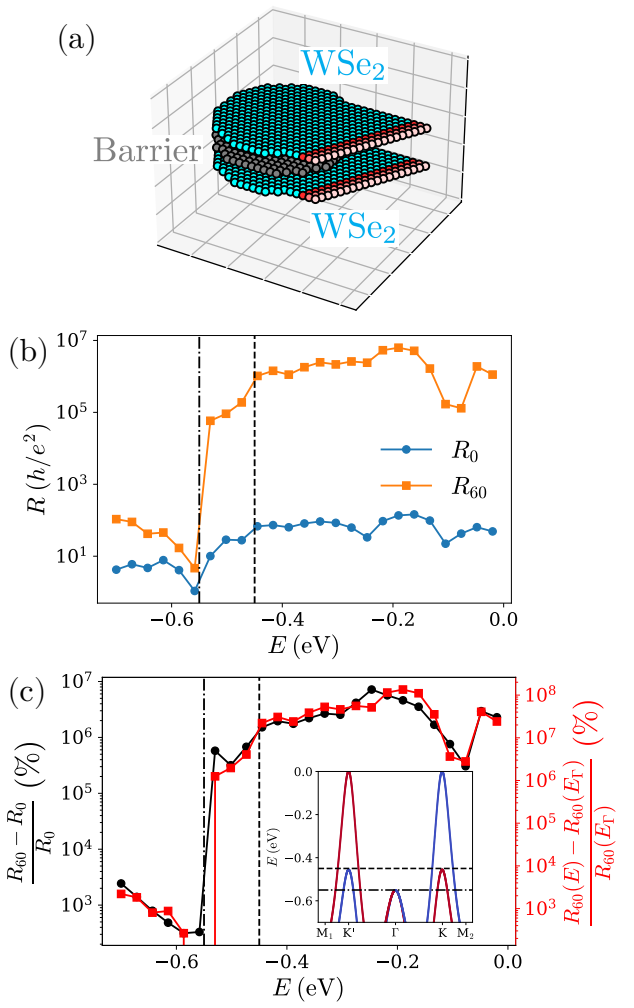

FIG. 2. (a) Schematics of the tunnel junction. Spheres are the tight-binding sites with colors cyan, gray and red being WSe_2, the barrier and three unit cells of the semi-infinite leads, respectively. Both the diameter L and the width of the leads are 20 nm, with a total number of over 10^4 sites in the scattering region. (b) Resistance as a function of energy for $\theta = 0°$ and $\theta = 60°$. (c) Switching resistance R_{sw} as a function of energy. Black line is R_{sw} between $\theta = 0°$ and $\theta = 60°$, and red line is R_{sw} for different energies at fixed angle $\theta = 60°$ with $R_{low} = R_{60}(E_\Gamma = -0.55)$. Inset: Band structure of the valence bands where the horizontal lines denote the energies at which other bands with opposite spin start contributing to transport. Such energies are also marked in the resistance plots in (b) and (c) as vertical lines.

As mentioned above, R_{60} changes abruptly near $E \sim -0.55$ eV. Therefore, at a fixed angle of $\theta = 60°$, one can define another switching resistance as a function of energy where R_{low} is taken at some energy right after the resistance drops, e.g. $(R_{60}(E) - R_{60}(-0.55))/R_{60}(-0.55)$. We plot this quantity as well in Fig. 2(c), and notice that

System	R_{sw} (%)	Magnetism	Mechanism	Year	Reference
CoFe/MgO/**CoFe**	~ 300	FM	Tunnel magnetoresistance	2004	[6]
Fe/MgO/**Fe**	~ 250	FM	Tunnel magnetoresistance	2004	[7]
NiFe/**IrMn**/MgO/Pt	~ 150	AFM	Tunnel anisotropic magnetoresistance	2011	[73]
FeRh	$\sim 0.1-1$	AFM	Anisotropic magnetoresistance	2014	[74]
CuMnAs	$\sim 0.1-1$	AFM	Anisotropic magnetoresistance	2016	[75]
graphite/**CrI_3**/graphite	$\sim 10^4$	2D magnet	AFM-FM transition	2018	[21]
graphite/**CrI_3**/graphite	~ 500	2D magnet	AFM-FM transition	2018	[22]
Fe_3GeTe_2/hBN/**Fe_3GeTe_2**	~ 160	2D FM	Tunnel magnetoresistance	2018	[23]
graphite/**CrI_3**/graphite	~ 500	2D magnet	AFM-FM transition	2018	[24]
graphite/**CrI_3**/graphite	$\sim 10^6$	2D magnet	AFM-FM transition	2018	[25]
Mn_3Pt/MgO/**Mn_3Pt**/MnPt/$MgAl_2O_4$	~ 100	NC-AFM	Tunnel magnetoresistance	2023	[54]
Mn_3Sn/MgO/**Mn_3Sn**	~ 2	NC-AFM	Tunnel magnetoresistance	2023	[55]

TABLE I. List of experimental switching resistances based on spin-dependent transport in representative systems. FM, AFM and NC-AFM stand for ferromagnetism, antiferromagnetism and noncollinear antiferromagnetism, respectively. The materials highlighted in bold denote the materials whose magnetic state is responsible for the switching process.

R_{sw} also surpasses $10^6\%$, implying that electrical tuning of the Fermi level could also be used to obtain large switching resistances. From the different TMDs studied [72], MoS_2 is the most promising candidate for such switching, as the Γ point appears only at $E \sim -0.065$ eV. Also, although our model only captures the spin splitting of the valence band, this effect could be achieved in the conduction band where the spin splitting is known to be of the order of tens of meV [70, 76], thus easily gate tunable.

Although the basic concept of this work compares the resistance between TMD bilayers with the same and opposite sign of spin-valley locking, one may wonder how the resistance transitions from 0 to 60 degrees. To elucidate such nontrivial trend, we calculate the resistance as a function of both energy and twist angle, and plot the results in Fig. 3. From these data, along with other different devices and models presented in the SM [72], we can discern few general trends from particular features of each model. Firstly, the resistance increases nonmonotonically until it reaches its maximum at 60°, independently of the energy. Secondly, while there are sudden jumps in resistance at different twist angles and energies, two major and characteristic resistance increases are identified at or near 0° and between 10° and 30° depending on the energy (see green line in Fig. 3(b)). The former one highlights the importance of momentum conservation and band alignment in the vertical transport, as small deviations from perfect alignment can result in dramatic changes in resistance. The latter variation is related to the size of Fermi surfaces and occurs when the top and bottom Fermi surfaces do not overlap in momentum space anymore, leading to a sudden increment in resistance. Since the Fermi surface increases with energy (away from the valence band maximum), the angle to reach that condition increases as well. The relationship between this angle and energy can be easily calculated [72], resulting in the green line shown in Fig. 3(b) which agrees very well with the numerical calculations of the resistance. The implication of such an effect is that, although the resistance is high at 60° irrespective of the energy, it grows faster at low energies. For instance, it reaches values of $10^4\ h/e^2$ as soon as $\theta \sim 15°$ for $E \sim -0.2$ eV, while it takes up to $\theta \sim 30°$ to reach similar values for $E \sim -0.4$ eV.

Finally, it is known that crystallinity and absence of scattering in the barrier helps conserve momentum and vertical transport [6, 7, 15]. Indeed, scattering in the metal-barrier interface is important as that can couple states with different momentum (and same spin) and reduce R_{sw}. Importantly for us, not all kinds of disorder will affect R_{sw} in the same manner. Long-range disorder will induce scattering involving small momentum changes, i.e. intra-valley scattering. This type of disorder should not severely impact R_{sw}. On the other hand, short-range scatterers, such as adatoms or vacancies, can mix states far away in the Brillouin zone and therefore produce inter-valley scattering that allow vertical transport even when the TMDs are not aligned. To unveil the dependency of inter-valley scattering on the switching resistance, we model vacancies in our system. To that end, we randomly remove sites in the tight-binding model (both TMDs and barrier) by associating a finite probability for the site to be eliminated [77, 78]. We relate this probability with the vacancy concentration and average over several vacancy configurations. In Fig. 4, we plot R_{sw} as a function of vacancy concentration at $E = -0.2$ eV. Clearly, R_{sw} quickly decreases with increasing concentration. However, experiments have shown that typical defect concentration in TMDs ranges $\sim 3\%$ [79–82], and for that value, R_{sw} is still large with value $\sim 10^4\%$. This suggests that ultraclean TMD tunnel junctions are

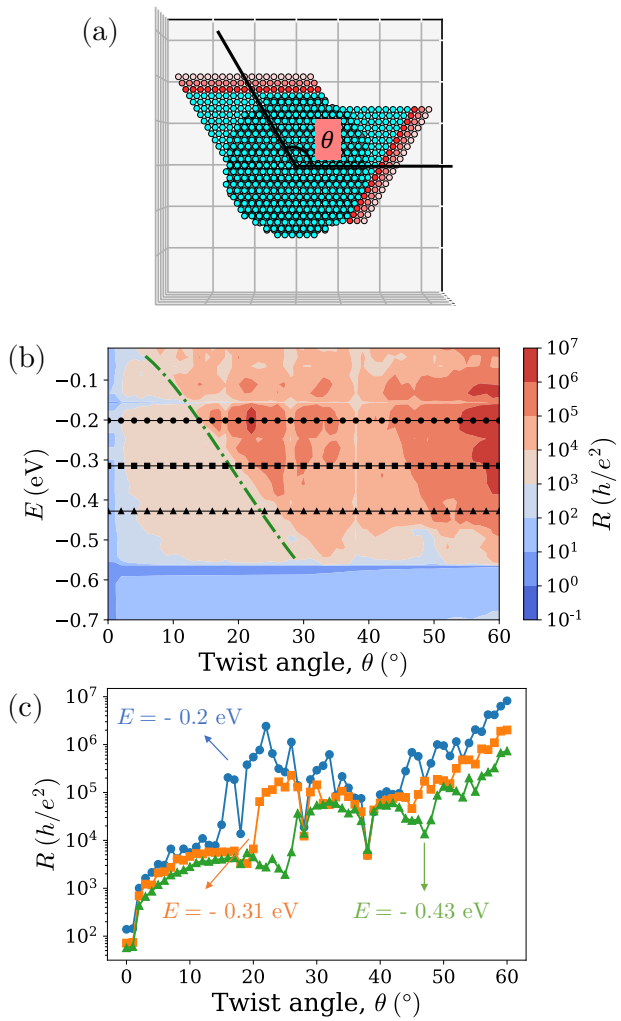

FIG. 3. (a) Top-view schematics of the tunnel junction with arbitrary twist angle θ. (b) Resistance as a function of energy and twist angle for the same device in Fig. 2. The green line marks the calculated angle after which the two Fermi surfaces do not overlap anymore. (c) Resistance as a function of twist angle for three selected energies, $E = -0.2$ eV, -0.31 eV, -0.43 eV, marked with lines in panel (b).

not needed to experience the $R_{\rm sw}$ reported here. In the SM [72], we substantiate this result by modelling other interfaces, like a different lattice for the tunnel barrier and with varying tight-binding parameters. In all cases, while the switching resistance is smaller than that of Fig. 2, emphasizing the importance of a clean interface to achieve a large $R_{\rm sw}$, they all show qualitatively similar behaviors, indicating that this mechanism of switching resistance is nevertheless expected despite material imperfections.

Discussion — We have revealed a spin-dependent switching resistance in a system without magnetic order. Such hitherto unprecedented phenomena originates from the effective tuning of SOC in TMD bilayers with

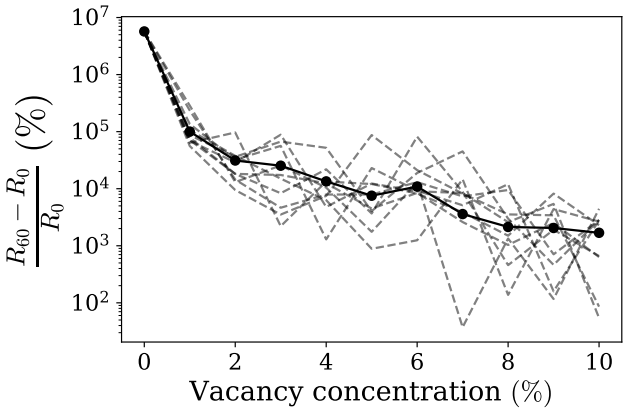

FIG. 4. (a) Switching resistance $R_{\rm sw}$ as a function of vacancy concentration at $E = -0.2$ eV. Solid line is the average performed over 10 disorder realizations (shown in dashed, paler color).

twist angle. Carefully tuning the twist angle between TMD monolayers allows to control the relative sign of the spin-valley locking between layers, achieving in this way low and high resistance states in vertical transport depending on the relative orientation of the TMDs. The efficiency of the resistance switch is above 10^6%, making it orders of magnitude larger than traditional magnetic tunnel junctions.

Motivated by the fascinating physics of moiré materials [34, 83], nanoscale control of twist angles in van der Waals heterostructures has seen a major development in recent years [64–66]. Specifically, the multiple works demonstrating sliding ferroelectricity in TMDs [84–86] suggest that our proposal device should be within current experimental reach, while the quantum twisting microscope offers the perfect setup to measure tunnel currents as a function of twist angle in TMD tunnel junctions [65]. Because of the large spin-orbit and spin splitting, the resistance switching should persist at room temperature, which should facilitate its experimental identification. Overall, our work puts forward a pioneering way to create next-generation memory and electronic devices based on twist angle engineering.

M. V. is grateful to Hossein Taghinejad, Joel E. Moore, Philip Kim, Daniel E. Parker, Tiancong Zhu and Michael F. Crommie for stimulating discussions. M.V. was supported as part of the Center for Novel Pathways to Quantum Coherence in Materials, an Energy Frontier Research Center funded by the US Department of Energy, Office of Science, Basic Energy Sciences.

* marcvila@berkeley.edu, mvilatusell@lbl.gov

[1] Z. Wang, H. Wu, G. W. Burr, C. S. Hwang, K. L. Wang, Q. Xia, and J. J. Yang, Nature Reviews Materials **5**, 173

(2020).
[2] M. Lanza, A. Sebastian, W. D. Lu, M. L. Gallo, M.-F. Chang, D. Akinwande, F. M. Puglisi, H. N. Alshareef, M. Liu, and J. B. Roldan, Science **376**, eabj9979 (2022), https://www.science.org/doi/pdf/10.1126/science.abj9979.
[3] M. Y. Zhuravlev, R. F. Sabirianov, S. S. Jaswal, and E. Y. Tsymbal, Phys. Rev. Lett. **94**, 246802 (2005).
[4] V. Garcia and M. Bibes, Nature Communications **5**, 4289 (2014).
[5] J. S. Moodera, L. R. Kinder, T. M. Wong, and R. Meservey, Phys. Rev. Lett. **74**, 3273 (1995).
[6] S. S. P. Parkin, C. Kaiser, A. Panchula, P. M. Rice, B. Hughes, M. Samant, and S.-H. Yang, Nature Materials **3**, 862 (2004).
[7] S. Yuasa, T. Nagahama, A. Fukushima, Y. Suzuki, and K. Ando, Nature Materials **3**, 868 (2004).
[8] R. Waser and M. Aono, Nature Materials **6**, 833 (2007).
[9] M. Lanza, H.-S. P. Wong, E. Pop, D. Ielmini, D. Strukov, B. C. Regan, L. Larcher, M. A. Villena, J. J. Yang, L. Goux, A. Belmonte, Y. Yang, F. M. Puglisi, J. Kang, B. Magyari-Kpe, E. Yalon, A. Kenyon, M. Buckwell, A. Mehonic, A. Shluger, H. Li, T.-H. Hou, B. Hudec, D. Akinwande, R. Ge, S. Ambrogio, J. B. Roldan, E. Miranda, J. Sue, K. L. Pey, X. Wu, N. Raghavan, E. Wu, W. D. Lu, G. Navarro, W. Zhang, H. Wu, R. Li, A. Holleitner, U. Wurstbauer, M. C. Lemme, M. Liu, S. Long, Q. Liu, H. Lv, A. Padovani, P. Pavan, I. Valov, X. Jing, T. Han, K. Zhu, S. Chen, F. Hui, and Y. Shi, Advanced Electronic Materials **5**, 1800143 (2019), https://onlinelibrary.wiley.com/doi/pdf/10.1002/aelm.201800143.
[10] W. H. Butler, X.-G. Zhang, T. C. Schulthess, and J. M. MacLaren, Phys. Rev. B **63**, 054416 (2001).
[11] J. Mathon and A. Umerski, Phys. Rev. B **63**, 220403 (2001).
[12] B. Dieny and M. Chshiev, Rev. Mod. Phys. **89**, 025008 (2017).
[13] L. Zhang, J. Zhou, H. Li, L. Shen, and Y. P. Feng, Applied Physics Reviews **8**, 021308 (2021), https://pubs.aip.org/aip/apr/article-pdf/doi/10.1063/5.0032538/14576861/021308_1_online.pdf.
[14] C.-W. Cheng, K.-M. Chen, J.-H. Wei, Y.-C. Hsin, S.-S. Sheu, C.-I. Wu, and Y.-C. Tseng, Journal of Physics D: Applied Physics **55**, 195002 (2022).
[15] E. Tsymbal, K. Belashchenko, J. Velev, S. Jaswal, M. van Schilfgaarde, I. Oleynik, and D. Stewart, Progress in Materials Science **52**, 401 (2007), modelling electrons and atoms for materials science.
[16] J. D. Burton and E. Y. Tsymbal, Phys. Rev. Lett. **106**, 157203 (2011).
[17] A. K. Geim and I. V. Grigorieva, Nature **499**, 419 (2013).
[18] F. Hui, E. Grustan-Gutierrez, S. Long, Q. Liu, A. K. Ott, A. C. Ferrari, and M. Lanza, Advanced Electronic Materials **3**, 1600195 (2017), https://onlinelibrary.wiley.com/doi/pdf/10.1002/aelm.201600195.
[19] H. Yang, S. O. Valenzuela, M. Chshiev, S. Couet, B. Dieny, B. Dlubak, A. Fert, K. Garello, M. Jamet, D.-E. Jeong, K. Lee, T. Lee, M.-B. Martin, G. S. Kar, P. Sénéor, H.-J. Shin, and S. Roche, Nature **606**, 663 (2022).
[20] F. Xue, Y. Ma, H. Wang, L. Luo, Y. Xu, T. D. Anthopoulos, M. Lanza, B. Yu, and X. Zhang, Matter **5**, 1999 (2022).
[21] T. Song, X. Cai, M. W.-Y. Tu, X. Zhang, B. Huang, N. P. Wilson, K. L. Seyler, L. Zhu, T. Taniguchi, K. Watanabe, M. A. McGuire, D. H. Cobden, D. Xiao, W. Yao, and X. Xu, Science **360**, 1214 (2018).
[22] D. R. Klein, D. MacNeill, J. L. Lado, D. Soriano, E. Navarro-Moratalla, K. Watanabe, T. Taniguchi, S. Manni, P. Canfield, J. Fernndez-Rossier, and P. Jarillo-Herrero, Science **360**, 1218 (2018), https://www.science.org/doi/pdf/10.1126/science.aar3617.
[23] Z. Wang, D. Sapkota, T. Taniguchi, K. Watanabe, D. Mandrus, and A. F. Morpurgo, Nano Letters **18**, 4303 (2018).
[24] Z. Wang, I. Gutiérrez-Lezama, N. Ubrig, M. Kroner, M. Gibertini, T. Taniguchi, K. Watanabe, A. Imamoğlu, E. Giannini, and A. F. Morpurgo, Nature Communications **9**, 2516 (2018).
[25] H. H. Kim, B. Yang, T. Patel, F. Sfigakis, C. Li, S. Tian, H. Lei, and A. W. Tsen, Nano Letters **18**, 4885 (2018).
[26] X. Li, J.-T. Lü, J. Zhang, L. You, Y. Su, and E. Y. Tsymbal, Nano Letters **19**, 5133 (2019).
[27] J. Wu, H.-Y. Chen, N. Yang, J. Cao, X. Yan, F. Liu, Q. Sun, X. Ling, J. Guo, and H. Wang, Nature Electronics **3**, 466 (2020).
[28] Q. Wang, T. Xie, N. A. Blumenschein, Z. Song, J. C. Kotsakidis, A. T. Hanbicki, M. A. Susner, B. S. Conner, Q. Tan, S. H. Lee, Z. Mao, X. Ling, T. Low, J.-P. Wang, A. L. Friedman, and C. Gong, Matter **5**, 4425 (2022).
[29] A. Xie, H. Hao, C.-S. Liu, X. Zheng, L. Zhang, and Z. Zeng, Phys. Rev. B **107**, 115427 (2023).
[30] Y. Zhu, B. Chi, L. Jiang, X. Guo, Y. Yan, and X. Han, Phys. Rev. Appl. **20**, 034010 (2023).
[31] M. Liao, Z.-W. Wu, L. Du, T. Zhang, Z. Wei, J. Zhu, H. Yu, J. Tang, L. Gu, Y. Xing, R. Yang, D. Shi, Y. Yao, and G. Zhang, Nature Communications **9**, 4068 (2018).
[32] S. Zhang, A. Song, L. Chen, C. Jiang, C. Chen, L. Gao, Y. Hou, L. Liu, T. Ma, H. Wang, X.-Q. Feng, and Q. Li, Science Advances **6**, eabc5555 (2020), https://www.science.org/doi/pdf/10.1126/sciadv.abc5555.
[33] P. K. Srivastava, Y. Hassan, D. J. P. de Sousa, Y. Gebredingle, M. Joe, F. Ali, Y. Zheng, W. J. Yoo, S. Ghosh, J. T. Teherani, B. Singh, T. Low, and C. Lee, Nature Electronics **4**, 269 (2021).
[34] Y. Cao, V. Fatemi, S. Fang, K. Watanabe, T. Taniguchi, E. Kaxiras, and P. Jarillo-Herrero, Nature **556**, 43 (2018).
[35] Y. Cao, D. Rodan-Legrain, J. M. Park, N. F. Q. Yuan, K. Watanabe, T. Taniguchi, R. M. Fernandes, L. Fu, and P. Jarillo-Herrero, Science **372**, 264 (2021).
[36] M. Oh, K. P. Nuckolls, D. Wong, R. L. Lee, X. Liu, K. Watanabe, T. Taniguchi, and A. Yazdani, Nature **600**, 240 (2021).
[37] J. M. Park, Y. Cao, L.-Q. Xia, S. Sun, K. Watanabe, T. Taniguchi, and P. Jarillo-Herrero, Nature Materials **21**, 877 (2022).
[38] Y. Cao, V. Fatemi, A. Demir, S. Fang, S. L. Tomarken, J. Y. Luo, J. D. Sanchez-Yamagishi, K. Watanabe, T. Taniguchi, E. Kaxiras, R. C. Ashoori, and P. Jarillo-Herrero, Nature **556**, 80 (2018).
[39] X. Lu, P. Stepanov, W. Yang, M. Xie, M. A. Aamir, I. Das, C. Urgell, K. Watanabe, T. Taniguchi, G. Zhang, A. Bachtold, A. H. MacDonald, and D. K. Efetov, Nature **574**, 653 (2019).
[40] D. Wong, K. P. Nuckolls, M. Oh, B. Lian, Y. Xie, S. Jeon, K. Watanabe, T. Taniguchi, B. A. Bernevig, and A. Yazdani, Nature **582**, 198 (2020).
[41] P. Stepanov, I. Das, X. Lu, A. Fahimniya, K. Watanabe,

T. Taniguchi, F. H. L. Koppens, J. Lischner, L. Levitov, and D. K. Efetov, Nature **583**, 375 (2020).
[42] I. Das, C. Shen, A. Jaoui, J. Herzog-Arbeitman, A. Chew, C.-W. Cho, K. Watanabe, T. Taniguchi, B. A. Piot, B. A. Bernevig, and D. K. Efetov, Phys. Rev. Lett. **128**, 217701 (2022).
[43] M. Serlin, C. L. Tschirhart, H. Polshyn, Y. Zhang, J. Zhu, K. Watanabe, T. Taniguchi, L. Balents, and A. F. Young, Science **367**, 900 (2020).
[44] G. Chen, A. L. Sharpe, E. J. Fox, Y.-H. Zhang, S. Wang, L. Jiang, B. Lyu, H. Li, K. Watanabe, T. Taniguchi, Z. Shi, T. Senthil, D. Goldhaber-Gordon, Y. Zhang, and F. Wang, Nature **579**, 56 (2020).
[45] K. P. Nuckolls, M. Oh, D. Wong, B. Lian, K. Watanabe, T. Taniguchi, B. A. Bernevig, and A. Yazdani, Nature **588**, 610 (2020).
[46] P. Stepanov, M. Xie, T. Taniguchi, K. Watanabe, X. Lu, A. H. MacDonald, B. A. Bernevig, and D. K. Efetov, Phys. Rev. Lett. **127**, 197701 (2021).
[47] T. Li, S. Jiang, B. Shen, Y. Zhang, L. Li, Z. Tao, T. Devakul, K. Watanabe, T. Taniguchi, L. Fu, J. Shan, and K. F. Mak, Nature **600**, 641 (2021).
[48] J. Cai, E. Anderson, C. Wang, X. Zhang, X. Liu, W. Holtzmann, Y. Zhang, F. Fan, T. Taniguchi, K. Watanabe, Y. Ran, T. Cao, L. Fu, D. Xiao, W. Yao, and X. Xu, Nature **622**, 63 (2023).
[49] H. Park, J. Cai, E. Anderson, Y. Zhang, J. Zhu, X. Liu, C. Wang, W. Holtzmann, C. Hu, Z. Liu, T. Taniguchi, K. Watanabe, J.-H. Chu, T. Cao, L. Fu, W. Yao, C.-Z. Chang, D. Cobden, D. Xiao, and X. Xu, Nature **622**, 74 (2023).
[50] V. M. Karpan, G. Giovannetti, P. A. Khomyakov, M. Talanana, A. A. Starikov, M. Zwierzycki, J. van den Brink, G. Brocks, and P. J. Kelly, Phys. Rev. Lett. **99**, 176602 (2007).
[51] V. M. Karpan, P. A. Khomyakov, A. A. Starikov, G. Giovannetti, M. Zwierzycki, M. Talanana, G. Brocks, J. van den Brink, and P. J. Kelly, Phys. Rev. B **78**, 195419 (2008).
[52] D.-F. Shao, Y.-Y. Jiang, J. Ding, S.-H. Zhang, Z.-A. Wang, R.-C. Xiao, G. Gurung, W. J. Lu, Y. P. Sun, and E. Y. Tsymbal, Phys. Rev. Lett. **130**, 216702 (2023).
[53] J. Dong, X. Li, G. Gurung, M. Zhu, P. Zhang, F. Zheng, E. Y. Tsymbal, and J. Zhang, Phys. Rev. Lett. **128**, 197201 (2022).
[54] P. Qin, H. Yan, X. Wang, H. Chen, Z. Meng, J. Dong, M. Zhu, J. Cai, Z. Feng, X. Zhou, L. Liu, T. Zhang, Z. Zeng, J. Zhang, C. Jiang, and Z. Liu, Nature **613**, 485 (2023).
[55] X. Chen, T. Higo, K. Tanaka, T. Nomoto, H. Tsai, H. Idzuchi, M. Shiga, S. Sakamoto, R. Ando, H. Kosaki, T. Matsuo, D. Nishio-Hamane, R. Arita, S. Miwa, and S. Nakatsuji, Nature **613**, 490 (2023).
[56] D.-F. Shao, S.-H. Zhang, M. Li, C.-B. Eom, and E. Y. Tsymbal, Nature Communications **12**, 7061 (2021).
[57] L. Šmejkal, A. B. Hellenes, R. González-Hernández, J. Sinova, and T. Jungwirth, Phys. Rev. X **12**, 011028 (2022).
[58] L. Šmejkal, J. Sinova, and T. Jungwirth, Phys. Rev. X **12**, 031042 (2022).
[59] L. Šmejkal, J. Sinova, and T. Jungwirth, Phys. Rev. X **12**, 040501 (2022).
[60] A. Pulkin and O. V. Yazyev, Phys. Rev. B **93**, 041419 (2016).
[61] A. Hallal, 2D Materials **7**, 015005 (2019).
[62] A. Manchon, H. C. Koo, J. Nitta, S. M. Frolov, and R. A. Duine, Nature Materials **14**, 871 (2015).
[63] D. Xiao, G.-B. Liu, W. Feng, X. Xu, and W. Yao, Phys. Rev. Lett. **108**, 196802 (2012).
[64] R. Ribeiro-Palau, C. Zhang, K. Watanabe, T. Taniguchi, J. Hone, and C. R. Dean, Science **361**, 690 (2018), https://www.science.org/doi/pdf/10.1126/science.aat6981.
[65] A. Inbar, J. Birkbeck, J. Xiao, T. Taniguchi, K. Watanabe, B. Yan, Y. Oreg, A. Stern, E. Berg, and S. Ilani, Nature **614**, 682 (2023).
[66] J. Wang, A. Khosravi, A. Vanossi, and E. Tosatti, Rev. Mod. Phys. **96**, 011002 (2024).
[67] Z. Y. Zhu, Y. C. Cheng, and U. Schwingenschlögl, Phys. Rev. B **84**, 153402 (2011).
[68] T. Wang, M. Vila, M. P. Zaletel, and S. Chatterjee, Phys. Rev. Lett. **132**, 116504 (2024).
[69] A. M. Jones, H. Yu, J. S. Ross, P. Klement, N. J. Ghimire, J. Yan, D. G. Mandrus, W. Yao, and X. Xu, Nature Physics **10**, 130 (2014).
[70] G.-B. Liu, W.-Y. Shan, Y. Yao, W. Yao, and D. Xiao, Phys. Rev. B **88**, 085433 (2013).
[71] C. W. Groth, M. Wimmer, A. R. Akhmerov, and X. Waintal, New Journal of Physics **16**, 063065 (2014).
[72] See Supplemental Material for additional details about the implementation of the tunnel junction and complementary results on other TMDs and analysis of the tunnel barrier.
[73] B. G. Park, J. Wunderlich, X. Martí, V. Holý, Y. Kurosaki, M. Yamada, H. Yamamoto, A. Nishide, J. Hayakawa, H. Takahashi, A. B. Shick, and T. Jungwirth, Nature Materials **10**, 347 (2011).
[74] X. Marti, I. Fina, C. Frontera, J. Liu, P. Wadley, Q. He, R. J. Paull, J. D. Clarkson, J. Kudrnovský, I. Turek, J. Kuneš, D. Yi, J.-H. Chu, C. T. Nelson, L. You, E. Arenholz, S. Salahuddin, J. Fontcuberta, T. Jungwirth, and R. Ramesh, Nature Materials **13**, 367 (2014).
[75] P. Wadley, B. Howells, J. Železný, C. Andrews, V. Hills, R. P. Campion, V. Novák, K. Olejník, F. Maccherozzi, S. S. Dhesi, S. Y. Martin, T. Wagner, J. Wunderlich, F. Freimuth, Y. Mokrousov, J. Kuneš, J. S. Chauhan, M. J. Grzybowski, A. W. Rushforth, K. W. Edmonds, B. L. Gallagher, and T. Jungwirth, Science **351**, 587 (2016).
[76] K. Kośmider, J. W. González, and J. Fernández-Rossier, Phys. Rev. B **88**, 245436 (2013).
[77] J. M. Caridad, S. R. Power, M. R. Lotz, A. A. Shylau, J. D. Thomsen, L. Gammelgaard, T. J. Booth, A.-P. Jauho, and P. Bøggild, Nature Communications **9**, 659 (2018).
[78] M. Vila, J. H. Garcia, and S. Roche, Phys. Rev. B **104**, L161113 (2021).
[79] J. Hong, Z. Hu, M. Probert, K. Li, D. Lv, X. Yang, L. Gu, N. Mao, Q. Feng, L. Xie, J. Zhang, D. Wu, Z. Zhang, C. Jin, W. Ji, X. Zhang, J. Yuan, and Z. Zhang, Nature Communications **6**, 6293 (2015).
[80] S. Roy, W. Choi, S. Jeon, D.-H. Kim, H. Kim, S. J. Yun, Y. Lee, J. Lee, Y.-M. Kim, and J. Kim, Nano Letters **18**, 4523 (2018).
[81] H. Taghinejad, D. A. Rehn, C. Muccianti, A. A. Eftekhar, M. Tian, T. Fan, X. Zhang, Y. Meng, Y. Chen, T.-V. Nguyen, S.-f. Shi, P. M. Ajayan, J. Schaibley, E. J. Reed, and A. Adibi, ACS Nano **12**, 12795 (2018).
[82] S. M. Gali, A. Pershin, A. Lherbier, J.-C. Charlier, and

D. Beljonne, The Journal of Physical Chemistry C **124**, 15076 (2020).
[83] E. Y. Andrei, D. K. Efetov, P. Jarillo-Herrero, A. H. MacDonald, K. F. Mak, T. Senthil, E. Tutuc, A. Yazdani, and A. F. Young, Nature Reviews Materials **6**, 201 (2021).
[84] X. Wang, K. Yasuda, Y. Zhang, S. Liu, K. Watanabe, T. Taniguchi, J. Hone, L. Fu, and P. Jarillo-Herrero, Nature Nanotechnology **17**, 367 (2022).
[85] A. Weston, E. G. Castanon, V. Enaldiev, F. Ferreira, S. Bhattacharjee, S. Xu, H. Corte-León, Z. Wu, N. Clark, A. Summerfield, T. Hashimoto, Y. Gao, W. Wang, M. Hamer, H. Read, L. Fumagalli, A. V. Kretinin, S. J. Haigh, O. Kazakova, A. K. Geim, V. I. Fal'ko, and R. Gorbachev, Nature Nanotechnology **17**, 390 (2022).
[86] L. Roge, L. Wang, Y. Zhang, S. Cai, P. Wang, M. Chhowalla, W. Ji, and S. P. Lau, Science **376**, 973 (2022), https://www.science.org/doi/pdf/10.1126/science.abm5734.